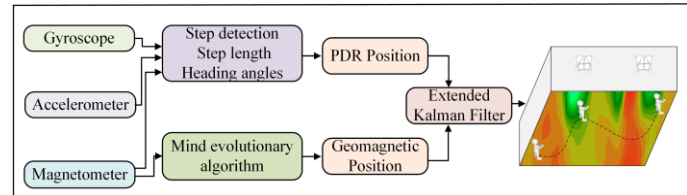


Indoor Localization Using Mind Evolutionary Algorithm-based Geomagnetic Positioning and Smartphone IMU Sensors

Meng Sun, Yunjia Wang, Wout Joseph and David Plets

Abstract— With the pervasiveness and ubiquitous distribution of the magnetic field in indoor environments, indoor localization using magnetic positioning (MP) has attracted considerable attention. This work concentrates on the MP and pedestrian dead reckoning (PDR) method, and constructs a fusion system for smartphones using MP and PDR based on the extended Kalman filter (EKF). The mind evolutionary algorithm (MEA) is introduced to search for the optimal magnetic position based on a heuristic searching strategy, which uses the similartaxis and dissimilation for the evolutionary operation. In the PDR module, the acceleration characteristics of different walking patterns are analyzed and the corresponding features are extracted. The enhanced genetic algorithm-based extreme learning machine (EGA-ELM) is adopted to train these features and address the gait recognition problem of different walking patterns. Finally, to obtain a lightweight and high-precision fusion method, MEA-based MP is integrated with PDR based on the EKF. Extensive experiments are conducted to evaluate the proposed methods. The testing results showed that MEA-based MP can obtain a location error within 2.3 m and steps can be recognized with a mean accuracy of 95% when different users participate in testing. The positioning results after fusion with PDR reveal that the mean location error and root-mean-square error (RMSE) are 1.25 m and 1.53 m respectively, which outperforms the MP, PDR, MP and PDR fusion methods using improved particle filter (IPF) and genetic particle filter (GPF).



Index Terms—Indoor positioning, sensor fusion, pedestrian dead reckoning (PDR), magnetic positioning, extended Kalman filter, mind evolutionary algorithm, magnetic field

I. INTRODUCTION

LOCATION-based services (LBS) are playing an increasingly important role in our modern society. Global navigation satellite systems (GNSSs) [1] provide meter-level location services but cannot work well in indoor environments. Indoor positioning system (IPS) utilizes different environment features to satisfy people's indoor LBS demands. Different IPSs have been studied, such as the wireless signal-based methods using WiFi signals [2], [3], Bluetooth [4], pseudolites [5], UWB [6], RFID [7], Zigbee [8], and the image-based methods including the visual positioning [9] and simultaneous localization and mapping [10]. To realize these approaches, developers should deploy signal transmitters or image targets in the environment and construct the radio map or measure the distance to perform positioning. With the high sensor integration of smartphones, performing localization on phones with WiFi or Bluetooth modules is feasible [11]. However, the wireless signal-based

method is complicated by an often-limited signal coverage and the complexity of the indoor topology [3]. Deploying more signal base stations may solve the coverage problem but will lead to larger deployment costs. UWB is more accurate than WiFi or Bluetooth, but it has a high energy consumption and requires the deployment of an additional infrastructure. The image-based method relies on an image database and the matching algorithm is usually complex. Labor-intensive image database construction and complicated positioning algorithms make it difficult to realize on terminals.

Apart from these, sensors like gyroscopes, accelerometers and magnetometers are also utilized for positioning. Pedestrian dead reckoning (PDR) [12] is such a method based on these sensors and can temporarily output high-precision positions. It is feasible to perform PDR on terminals without considering wireless signal coverage or infrastructure costs. However, PDR suffers from various measurement errors in the heading angle, step detection, and step length estimation, which will lead to large deviations in the PDR-derived positions over time. Only using PDR may not deliver precise results. Researchers usually integrate PDR with other technologies to reduce errors, like combining Wi-Fi in [13], Bluetooth in [14], and WiFi/scene recognition in [15]. Compared with the above methods, PDR is consequent, infrastructure-free, and it is the preferred solution for fusion positioning.

As a solution for the cost investment and signal coverage problems, researchers have found that the magnetic field (MF) is ubiquitous and spatially discernible [16], [17], and can be used for positioning. The theory of magnetic positioning (MP)

This work was supported by the National Key Research and Development Program of China under Grant 2016YFB0502102, in part by the China Scholarship Council under Grant CSC 202006420023, in part by the Postgraduate Research & Practice Innovation Program of Jiangsu Province under Grant KYCX21_2293. (Corresponding author: Yunjia Wang)

Meng Sun and Yunjia Wang are with the Key Laboratory of Land Environment and Disaster Monitoring, MNR, School of Environment and Spatial Informatics, China University of Mining and Technology, Xuzhou 221116, China (e-mail: msun@cumt.edu.cn; wjyc411@163.com).

David Plets and Wout Joseph are with the IMEC-WAVES Group, Department of Information Technology, Ghent University, Ghent, 9052, Belgium. (e-mail: David.Plets@ugent.be; Wout.Joseph@ugent.be).

is to collect the MF features of the environment and construct the MF database for online positioning. Based on our literature review, we divide the previous works into two categories, which are sequence-based magnetic positioning (SBMP) and single-point-based magnetic positioning (SPMP). SBMP uses magnetic sequences to realize localization and the positioning algorithms include Gauss-Newton iteration [18], dynamic time wrapping (DTW) [19], convolutional neural network (CNN) [20], and recurrent neural network (RNN) [21]. However, SBMP is not flexible because testers must walk along the planned paths to obtain positions. Oppositely, SPMP is more flexible. It uses magnetic features at reference points without considering the walking paths. Positioning algorithms like the k-nearest neighbors (KNN) [22], stochastic magnetic matching [23], etc., have been extensively studied. The weakness of SPMP is accuracy, which is caused by the low-dimensional magnetic features. To improve precision, a particle filter (PF) is usually applied to SPMP, and researches in [24, 25] have proved that performing SPMP using PF could obtain good performance. Particle degradation is an inevitable problem of PF and it still exists even when applying resampling methods. PF also needs lots of particles to optimize particle degradation, which leads to high consumption of computing resources. Because of the high sampling rate of a magnetometer (e.g. 50Hz), numerous magnetic positions will be generated within one second, making it necessary to adopt a good algorithm to find the optimal value from these results while accounting for the algorithm complexity.

From the PDR prospect, most previous works concentrate on the implementation by holding the terminals horizontally and walking forward continuously. A larger error will be introduced if the tester walks backward or laterally because the position is still updated forward in these cases (e.g. tracking of a drone operator in warehouses walking forward/backward/sideways while looking at the drone). Therefore, it is necessary to recognize the walking patterns of pedestrians taking steps. To address these problems, we devised different methods to solve them. Our contributions can be summarized as follows:

- 1) We concentrate on the low-accuracy problem of SPMP and propose a novel SPMP based on the mind evolutionary algorithm (MEA). The optimal geomagnetic position can be quickly obtained from a series of candidate positions using the MEA's heuristic searching strategy.
- 2) We analyze the acceleration characteristics of different walking patterns and propose to combine the acceleration components for step recognition based on the enhanced genetic algorithm-based extreme learning machine (EGA-ELM). This lightweight step identification algorithm can accurately detect steps and make PDR error-tolerant to step detection failure under different walking patterns.
- 3) We construct an EKF-based fusion system that integrates the MEA-based MP and PDR. Testing results show that the proposed method can provide satisfactory fusion positions and outperforms the state-of-the-art approaches fusing MP and PDR based on the improved particle filter (IPF) and genetic particle filter (GPF).

The remainder of this paper is organized as follows. Section II discusses related works. Section III presents the architecture of the proposed methods. Section IV provides the experimental

analysis and discussion. Section V draws the conclusions.

II. RELATED WORKS

A. Geomagnetic Positioning

The geomagnetic field derived from the indoor buildings is spatially discernible as reported in [16] and it can be regarded as a signal source for positioning. Since Suksakulchai *et al* [17] first pointed it out and conducted location experiments, many types of research have been performed. These works can be divided into SBMP and SPMP.

1) Sequence-based magnetic positioning

SBMP utilizes the magnetic field sequence (MFS) and needs to plan the routes in the positioning area and collects the MFS along these paths. After that, sequence similarity assessment algorithms are adopted for positioning. For instance, the DTW algorithm was used for MFS matching to recognize hallways in [26] and a high-precision recognition rate provided a solid foundation for their research in [19], where they proposed a "LocateMe" system. In [12], integrating DTW-based SBMP with robust PDR is proposed and obtains an accuracy within 1.22 m in 75% of the cases. In [27], DTW-based SBMP combining WiFi-based tracking leads to a positioning precision of 3.5 m in 90% of the cases. These works proved that DTW can achieve a good performance, but its complexity is relatively high. Apart from the DTW algorithm, another SBMP method called "Gauss-Newton iteration" (GNI) was proposed in [18]. It gathers the magnetic field data along the tester's trajectory to construct pieces of MFSs and uses the GNI method to find the optimally aligned reference MFS. Their experiments show that integrating PDR with SBMP can obtain a localization error within 2.34 m. Moreover, Ashraf *et al* [28] proposed to store the magnetic patterns using the concept of the binary grid (BG), and obtained an accuracy of 4 m in 75% of the cases by fusing BG-based SBMP with PDR. They also presented the "GUIDE" system in [29], which can localize a pedestrian within 1.93 m in 90% of the cases. There are also other learning algorithms used for SBMP. In [20], the CNN is adopted for the "MINLOC" model and could localize a user within 1.01 m in 75% of the cases. In [21], testers used an RNN model and achieved an average localization accuracy of 1.04 m. In [30], a deep recurrent neural network (DRNN) was used and an overall magnetic landmarks classification accuracy of 97.2% was obtained. These works have shown that SBMP can obtain promising results. However, due to the randomness of walking and the algorithm complexity, SBMP may not perform well in real scenarios.

2) Single-point-based magnetic positioning

SPMP is more flexible compared with SBMP because it just uses the magnetic features at the reference points. Basically, the KNN method is often used to measure similarity and research work in [31] adopted the KNN to carry out experiments on the walkway and obtained good results. In [23], researchers proposed the stochastic magnetic matching (MM) algorithm by using the massive crowdsourced magnetic features, delivering location errors within 2 m. In [32], the multi-magnetic-

fingerprint-fusion (MMFF) method was presented to match the magnetic fingerprint. The positioning error was within 1 m, but the test area was not large. Similarly, the least-square method (LSM) and the improved mean square difference (MSD) were introduced in [33]. These two methods for MM obtained an overall accuracy of 1.2 m. To improve localization accuracy, a particle filter (PF) is very popular in both MM and fusion positioning. The general idea is to find the best position estimation from many particles. In [22], a KNN-based SPMP is integrated with PDR based on a genetic particle filter (GPF) and obtains a mean accuracy of 1.72 m. Xie *et al* [24] used magnetic features as observations to update the particle weights of the reliability-augmented PF and obtained an average accuracy of 1~2.8 m in a large building by integrating the PDR method. In [25], Zheng *et al* introduced the sensitivity-based adaptive PF based on the relationships between the target positions and magnetic maps, and the location error is within 2.02 m. To solve filter divergence and accelerate convergence, an improved PF (IPF) based on initial positioning error constraint was proposed in [34] and experiments showed that the effectiveness and reliability of PF were improved. In [35], a tracking system using SPMP and PDR based on an IPF was presented and the fusion precision was about 1.8 m in 90% of the cases. All these works have shown the good performance of fusion positioning using PF. However, the large execution time and particle degradation problem cannot be avoided even if some resampling methods are used. Moreover, PF finally uses the averaged resampled particles as the filtered result and that may introduce errors in positions. In addition to PF, there needs to adopt a good algorithm for SPMP while accounting for the positioning accuracy and algorithm complexity.

B. Pedestrian Steps Recognition

Different strategies are proposed to solve step recognition problems that are inherent to the use of PDR. For instance, the auto-correlation coefficient and standard deviation of the acceleration are calculated and used for step counting in [2]. Results showed this algorithm performed well when the tester was stationary or walking forward. Aiming at the same problem, the multi-threshold step detection algorithm based on the peak-valley detection constraints was presented in [14], where the peaks, valleys of the acceleration and time difference were used. This algorithm was more robust, and the moving states (walking forward and running) could be accurately recognized. In [18], the inertial navigation system (INS) based PDR that uses the zero-velocity update technology (ZUPT) to address the step detection failure problem was adopted, and the results showed INS-based PDR outperformed the gait-based PDR. In [24], a dynamic step length estimation method was proposed, and can adaptively estimate traveled distance. Testing results also revealed this method made their MP system error-tolerant in step detection. Besides, the artificial neural network (ANN) was selected for the gait identification in the magnetic fusion system in [28], the static and walking detection accuracy was 95% by using gyroscope data. Moreover, a walking pattern-based step detection method based on the multi-head CNN was proposed in [12], and the recognition rate was more than 98%. An adaptive four-threshold step detection (ATD) algorithm was proposed in [35] by using the acceleration thresholds and time intervals, an overall detection accuracy of 98% was obtained by

walking forward along the testing path. These works confirm that step detection failure leads to error accumulation of PDR. The pedestrian's walking process is uncertain and may contain backward or lateral movements during the whole process. This factor makes step identification more complicated. Although the CNN model in [12] shows good performance in the gait recognition of different walking patterns, realizing CNN on terminals is challenging. An effective step detection method is necessary to be studied regarding the algorithm complexity and more walking patterns.

To address the above-mentioned problems, this work adopts a heuristic mind evolutionary algorithm (MEA) to optimize the low-accuracy problem of SPMP. This MEA-based SPMP can quickly search for the optimal magnetic position in the space. The enhanced genetic algorithm-based extreme learning machine (EGA-ELM) is utilized to address the step detection problem of different walking patterns. Finally, a fusion localization system is constructed using the MEA-based SPMP and PDR based on the EKF.

III. MATERIALS AND METHODS

A. Pedestrian Dead Reckoning Module

PDR method estimates walking steps, moving directions, and step length based on the inertial measurement units (IMU) embedded in smartphones. However, step detection failure caused by different walking patterns leads to serious error accumulation on PDR positions. As Fig.1 shows, if one user moves backward from B to A (the phone's direction is from A to B), the classic PDR still considers the walking process as moving forward, and the position will be updated to F, but the user has returned to A. The same results occur when moving left to C or right to D. Therefore, it is necessary to identify the walking patterns when pedestrians take steps.

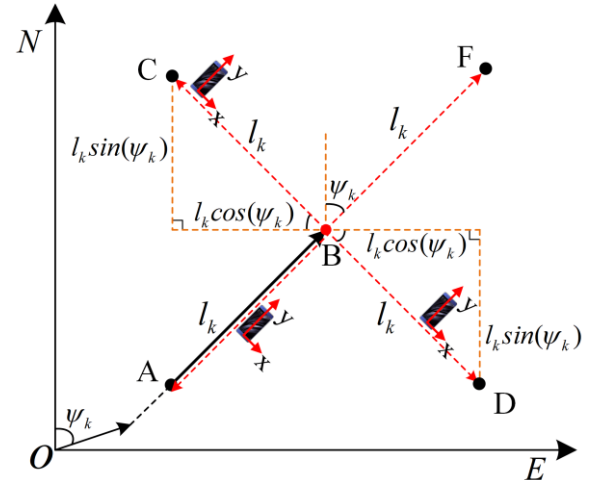


Fig. 1. PDR positions update under different walking patterns.

Considering the walking patterns and the geometric relationship in Fig.1, the producer of PDR in this work is shown in Fig.2 and the position update equation is defined as follows:

$$\begin{bmatrix} N_{k+1} \\ E_{k+1} \\ l_{k+1} \end{bmatrix} = \begin{bmatrix} 1 & 0 & f_k \cos \psi_k - \beta_k \sin \psi_k \\ 0 & 1 & f_k \sin \psi_k + \beta_k \cos \psi_k \\ 0 & 0 & 1 \end{bmatrix} \begin{bmatrix} N_k \\ E_k \\ l_k \end{bmatrix} + \begin{bmatrix} \sigma_1 \\ \sigma_2 \\ \Delta l \end{bmatrix} \quad (1)$$

where (N_k, E_k) represents the pedestrian location at the time k ,

l_k and ψ_k are the step length and heading angles, σ_1 and σ_2 are the system errors on N_k and E_k , Δl is the step length variation, respectively; f_k indicates walking forward or backward, and β_k indicates moving left or right. When moving forward or backward, f_k is set to 1 or -1, and β_k is set to 0, respectively. When moving left or right, β_k is set to -1 or 1, and f_k is set to 0, respectively. Equation (1) can also be defined as:

$$X_{k+1} = \Phi \cdot X_k + W_k \quad (2)$$

where X_k and X_{k+1} represent the PDR positions at the time k and $k+1$, Φ and W_k correspond to the matrixes in (1).

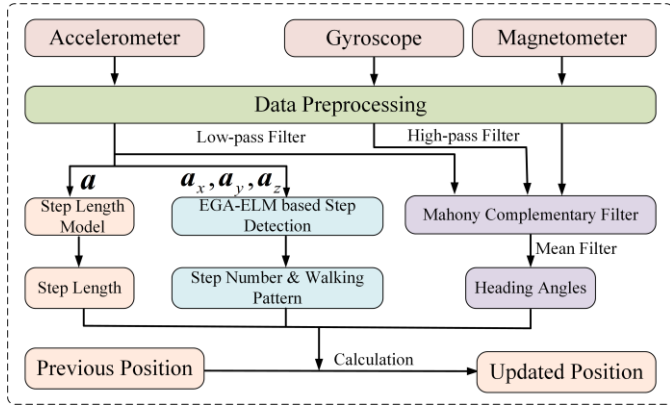


Fig. 2. Flowchart of PDR module in this work.

1) Heading angle estimation

The heading angle, also known as the yaw, is the angle between the pedestrian's walking direction and the north. Many estimation methods have been studied, such as gyroscope-based heading estimation [36], magnetometer-based algorithms [37], sensor fusion [38], and machine learning-based methods [39]. To take full advantage of smartphone IMU sensors data, the Mahony complementary filter (MCF) [40] is adopted in this work. MCF uses the gyroscope to calculate heading angles while the accelerometer and magnetometer will compensate the gyroscope's drift errors in time. The calculation producer mainly uses quaternion, and the quaternion is updated by using the sensors data. The initial quaternion vector is expressed as:

$$Q = [q_0 \ q_1 \ q_2 \ q_3]^T \quad (3)$$

The values of Q are updated based on the gyroscope data and error compensation items, which are expressed as:

$$e = e_a + e_m \quad (4)$$

where e_a and e_m are calculated by using filtered accelerometer and magnetometer data, respectively. The low pass filter [41] and high-pass filter [42] are applied to process the measured acceleration and magnetic data, respectively. The definitions of these two error terms are as follows:

$$\begin{cases} e_a = (C_n^b \cdot g_a) \times a \\ e_m = (C_n^b \cdot b_m) \times m \end{cases} \quad (5)$$

where ' \cdot ' represents the matrix multiplication and ' \times ' represents vector cross product, $g_a = [0 \ 0 \ g]^T$ is the standard gravity vector in the geographic coordinate system (GCS) and $g = 9.8m/s^2$; b_m is the geomagnetic vector when the x-axis of magnetometer points to the north of earth and $b_m = [b_{mx} \ 0 \ b_{mz}]^T$; a and m are the normalized measured acceleration and

geomagnetic data; C_n^b is the rotation matrix from the GCS to device coordinate system (DCS) [22]. These two error terms are utilized for the gyroscope error compensation as follows:

$$\omega = \omega_g + K_p e + K_I \int e \quad (6)$$

where ω and ω_g are the corrected and measured gyroscope data, and $\omega = [\omega_x \ \omega_y \ \omega_z]^T$, $\omega_g = [\omega_{gx} \ \omega_{gy} \ \omega_{gz}]^T$; K_p and K_I are the error control items. The compensated gyroscope data is then substituted into the quaternion differential equation and the first-order Runge-Kutta method [43] is adopted to solve this equation. The updated quaternion values are defined as follows:

$$\begin{cases} q_0(t+T) = q_0(t) - \frac{T}{2} [\omega_x q_1(t) + \omega_y q_2(t) + \omega_z q_3(t)] \\ q_1(t+T) = q_1(t) + \frac{T}{2} [\omega_x q_0(t) + \omega_z q_2(t) - \omega_y q_3(t)] \\ q_2(t+T) = q_2(t) + \frac{T}{2} [\omega_y q_0(t) - \omega_z q_1(t) + \omega_x q_3(t)] \\ q_3(t+T) = q_3(t) + \frac{T}{2} [\omega_z q_0(t) + \omega_y q_1(t) - \omega_x q_2(t)] \end{cases} \quad (7)$$

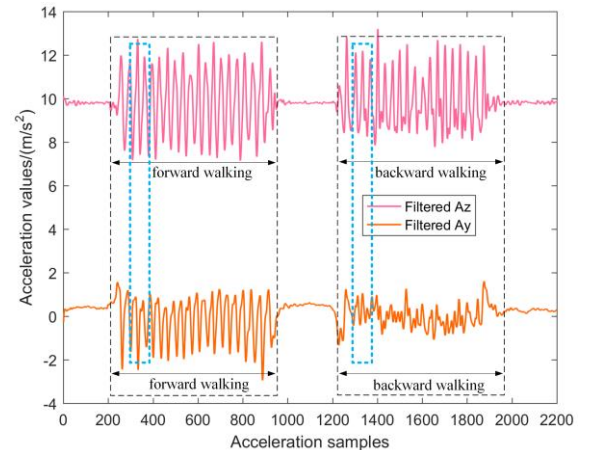
where T is the sampling time interval, $q_i(t)$ and $q_i(t+T)$ are the quaternion values at the time t and $(t+T)$. To estimate the heading angles, the updated quaternion values are normalized. The heading or yaw estimation equation is as follows:

$$\psi = \text{tg}^{-1} \frac{2(q_1 q_2 + q_0 q_3)}{1 - 2(q_2^2 + q_3^2)}, \quad \psi \in (0, 2\pi) \quad (8)$$

To reduce the influence of outliers, the mean filter algorithm is used to filter the raw estimated heading angles in one second and the filtered value is the estimated heading. In this work, 50 heading angles are generated and filtered in one second.

2) Walking pattern-based step detection

PDR positions are updated if one step is detected. Most existing algorithms mainly utilize z-axis acceleration or the modulus of 3-axis acceleration components to recognize steps because they vary with pedestrians' walking process. Detection algorithms like finite-state machine (FSM) [22], peak detection [44], zero velocity update method [18], etc., have been studied and perform well when people walk forward. However, position errors will be accumulated under backward or lateral walking because PDR still considers these updates as occurring in a forward movement. It is necessary to recognize the correct steps of different walking patterns. Therefore, we propose a novel step detection method by using an EGA-ELM in [45].



(a)

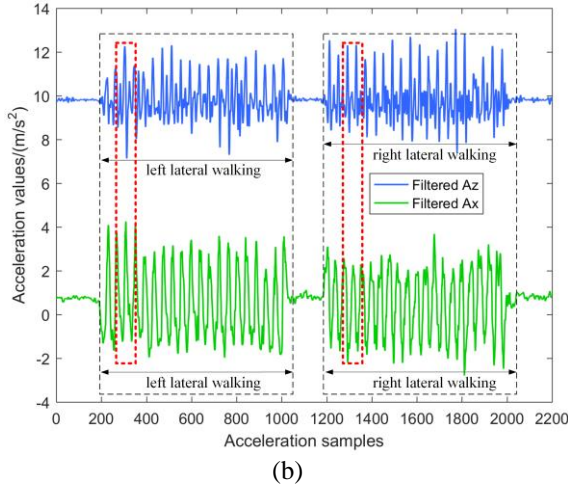


Fig. 3. Acceleration curves comparison of different movements. (a) forward and backward 20 steps; (b) left and right lateral 20 steps

Fig.3 shows that when moving forward, the filtered A_z and A_y vary with walking, but A_y doesn't show the same behavior under backward walking. When walking laterally, A_x shows a strong correlation with the walking process while A_z doesn't follow this. Therefore, it is concluded that moving forward or laterally can be recognized by using the 3-axis acceleration. We can combine A_z and A_y for backward and forward recognition, A_z and A_x for left and right walking detection. To implement EGA-ELM, the 3-axis acceleration is first normalized, and then divided into segments using a sliding window. If the window size is m , the partition process is expressed as follows:

$$I_i^x = (a_n^x, a_{n+1}^x, a_{n+2}^x, \dots, a_{n+m}^x) \quad (9)$$

$$I_i^y = (a_n^y, a_{n+1}^y, a_{n+2}^y, \dots, a_{n+m}^y) \quad (10)$$

$$I_i^z = (a_n^z, a_{n+1}^z, a_{n+2}^z, \dots, a_{n+m}^z) \quad (11)$$

Then, the training segments are constructed by integrating the I_i^z and I_i^y for the forward and backward movement, and using the I_i^z and I_i^x for the lateral movement. The detailed process is as follows:

$$\begin{cases} S_i = (I_i^z, I_i^y) = (a_n^z, a_{n+1}^z, a_{n+2}^z, \dots, a_{n+m}^z, a_n^y, a_{n+1}^y, a_{n+2}^y, \dots, a_{n+m}^y) \\ L_i = (I_i^z, I_i^x) = (a_n^z, a_{n+1}^z, a_{n+2}^z, \dots, a_{n+m}^z, a_n^x, a_{n+1}^x, a_{n+2}^x, \dots, a_{n+m}^x) \end{cases} \quad (12)$$

where S_i and L_i are the training segments for moving forward or backward, and right or left, respectively. The training labels for different movements and sliding window size in this work are referenced in Tab. I.

TABLE I
CONFIGURATION FOR LEARNING MODELS

Parameters explanation	Abbreviation	Labels or values
Forward movement	FM	1
Backward movement	BM	2
Left lateral movement	LLM	3
Right lateral movement	RLM	4
Sliding window size	SWS	50
Training segment length	TSL	100

3) Step length estimation

Various step length estimation models have been proposed, such as the constant model [46], linear model [47], nonlinear model [48], [49], and deep learning model [50]. In our work, the *Weinberg* model in [49] is adopted to calculate step length and its definition is as follows:

$$SL = K \sqrt{a_{max} - a_{min}} \quad (13)$$

where K is the scale factor and set to 0.5 in this work, a_{max} and a_{min} are the maximum and minimum of the acceleration during one step period.

B. Geomagnetic Positioning Module

1) Geomagnetic features extraction

The 3-axis magnetic field measured by smartphones is in the device coordinate system (DCS). Different phone attitudes will lead to different measurements. Therefore, it should transform the magnetic data to the geographic coordinate system (GCS), which is independent from the phone orientation. If the magnetic vector in the DCS is $B_D = [B_{D_x} \ B_{D_y} \ B_{D_z}]^T$ and $B_G = [B_{G_x} \ B_{G_y} \ B_{G_z}]^T$ is the vector in the GCS, the transformation is described as:

$$B_G = (C_n^b)^T B_D \quad (14)$$

where C_n^b is the rotation matrix from GCS to DCS, calculated as follows:

$$C_n^b = \begin{bmatrix} \cos \gamma & 0 & -\sin \gamma \\ 0 & 1 & 0 \\ \sin \gamma & 0 & \cos \gamma \end{bmatrix} \begin{bmatrix} 1 & 0 & 0 \\ 0 & \cos \theta & \sin \theta \\ 0 & -\sin \theta & \cos \theta \end{bmatrix} \begin{bmatrix} \cos \psi & -\sin \psi & 0 \\ \sin \psi & \cos \psi & 0 \\ 0 & 0 & 1 \end{bmatrix} \quad (15)$$

where γ , θ and ψ are the roll, pitch, and yaw angles of mobile phones. The definition of yaw angles is described in Section A, and the calculation methods of roll and pitch can be expressed as follows by using the quaternion values in (7):

$$\begin{cases} \theta = -\sin^{-1} 2(q_1 q_3 - q_0 q_2), \quad \theta \in (-\pi/2, \pi/2) \\ \gamma = \tan^{-1} \frac{2(q_2 q_3 + q_0 q_1)}{1 - 2(q_1^2 + q_2^2)}, \quad \gamma \in (-\pi, \pi) \end{cases} \quad (16)$$

After obtaining these three angles, the three stable magnetic features can be obtained using (14) and (15).

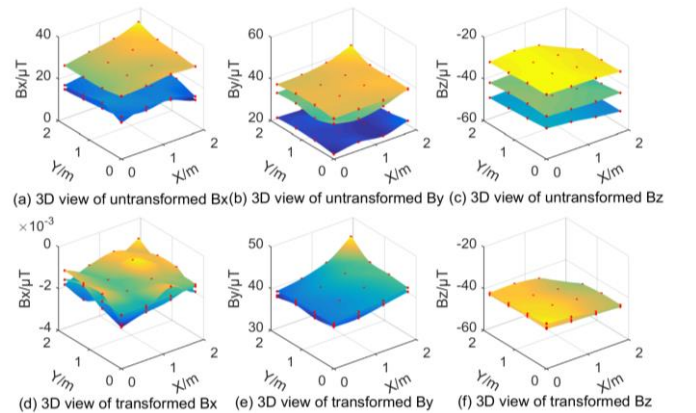


Fig. 4. Geomagnetic field transformation comparison of three attitudes.

Fig.4 reveals that, in the same area, the transformed 3-axis magnetic field data of three different postures are more stable than those of the untransformed data. It is not enough for high-precision positioning using only three features because the mismatching phenomenon appears frequently. Therefore, we

extracted the horizontal intensity B_h and total intensity B of the magnetic field and utilized five features for matching. Their definitions are as follows:

$$\begin{cases} B_h = \sqrt{B_x^2 + B_y^2} \\ B = \sqrt{B_x^2 + B_y^2 + B_z^2} \end{cases} \quad (17)$$

After obtaining these five magnetic features, we construct the fine-grained magnetic database by linearly interpolating the features and coordinates, and performing MEA for the accurate magnetic position estimation.

2) Mind evolutionary algorithm

The mind evolutionary algorithm (MEA) [51] is a popular method for searching and optimization problems, having a good optimizing performance and fast convergence speed. It emulates the learning modes and activities of the human mind and utilizes a groupization strategy to find the optimal solution. Similar with the genetic algorithm (GA) [52], MEA also has the evolutionary process but uses the similartaxis and dissimilation operators instead of selection, crossover, and mutation operations in GA. Crossover and mutation operation of GA may generate bad genes which affect the evolution process. However, similartaxis and dissimilation of MEA can work together while maintaining independence to improve search and optimization efficiency. MEA can also memorize every generation's evolutionary information and utilize this to guide the evolution toward the optimal direction.

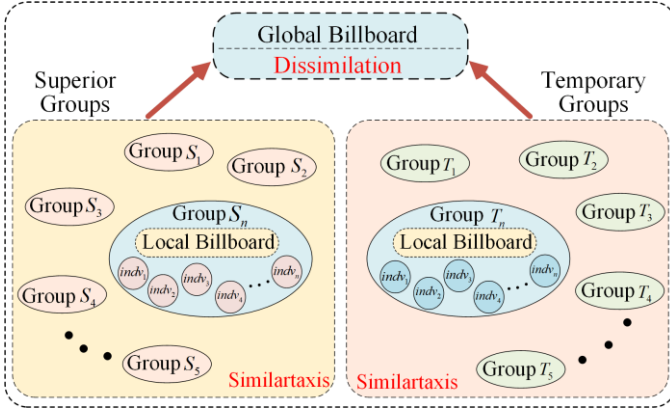


Fig. 5. The structure of mind evolutionary algorithm

As Fig.5 shows, the evolutionary process of MEA is as follows:

Step 1: Initialization. MEA first initializes a population with s superior subgroups and T temporary subgroups in the space. Every subgroup has its center and m uniformly distributed individuals around this center. Every individual is scored based on the adaptability to the searching space

Step 2: Similartaxis and local competition. The purpose of similartaxis is to make the subgroups mature by performing the local competition. The individuals within one group compete by comparing their scores. Good individuals are continuously generated and posted on the local billboard until the maximal and minimal scores within one group satisfy the mature condition. If one group is mature, the optimal individual and its score will be recorded on the global billboard.

Step 3: Dissimilation and global competition. If all groups

are mature, the dissimilation operation is executed to find the result based on the posted scores on the global billboard. These scores are compared and the superior group with a lower score is replaced by the temporary subgroup with a higher score. A new temporary subgroup will be generated in the space.

MEA performs these three steps until reaching the maximal iteration times or no superior subgroup is replaced. Finally, the optimal superior group or the optimal individual of the best superior group is selected as the searched result.

3) MEA-based geomagnetic positioning

Since the high sampling frequency (SF) of the magnetometer, many temporary geomagnetic positions (GP) can be generated within one second. These temporary GPs are used to form a population for MEA evolution. If the SF is n Hz and the population at the time k is $M(k)$, it can be expressed as:

$$M(k) = \{g_k(x_1, y_1), \dots, g_k(x_i, y_i), \dots, g_k(x_n, y_n)\} \quad (18)$$

where $g_k(x_i, y_i)$ is the i -th individual of $M(k)$, x_i and y_i are the coordinate values, $i=1,2,3,\dots,n$. Every individual's score is related to the previous magnetic position. If $G(k-1)=(X_{k-1}, Y_{k-1})$ is the position at the time $k-1$, the score can be calculated by:

$$score\{k, i\} = \frac{1}{\|G(k-1) - g_k(x_i, y_i)\|_2} \quad (19)$$

As Fig.6 shows, the first step of MEA is to initialize a population. The temporary GPs are scored using (19). The GPs with higher scores are selected as the superior groups' centers, and the ones with lower scores are selected as the temporary groups' centers. Individuals of the population are generated with random distribution around the centers, and are scored using (19). Then, MEA executes the similartaxis. Individuals within the same subgroup compete by comparing their scores. A subgroup is mature if the following condition is met:

$$|score_{max} - score_{min}| \leq \varepsilon \quad (20)$$

where ε is a threshold and set to 0.4 in this work, $score_{max}$ and $score_{min}$ are the maximal and minimal individuals' scores. If all the subgroups are mature, it goes to the third step: dissimilation operation and global competition. MEA executes similartaxis and dissimilation until meeting convergent conditions. The best individual with the largest score of the mature superior groups is selected as the final magnetic position.

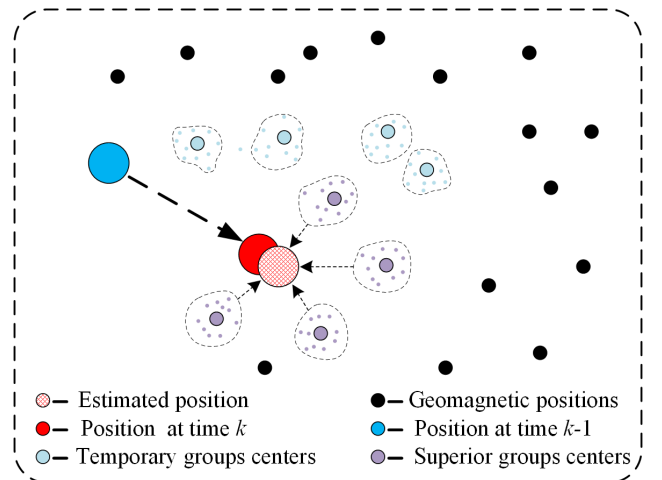


Fig. 6. Geomagnetic positions distribution.

C. Fusion Positioning Model

The system utilizes the output of the PDR as the system state and it will be corrected by the geomagnetic position. Based on the EKF theory, the integration model is expressed as follows:

$$\begin{cases} \mathbf{X}(k) = \mathbf{F} \cdot \mathbf{X}(k-1) + \mathbf{W}(k-1) \\ \mathbf{Z}(k) = \mathbf{H} \cdot \mathbf{G}(k) + \mathbf{V}(k) \end{cases} \quad (21)$$

where $\mathbf{X}(k)$ and $\mathbf{X}(k-1)$ are the PDR position vectors at the time k and $k-1$, $\mathbf{Z}(k)$ and $\mathbf{G}(k)$ are the systematic observation and geomagnetic position at the time k , respectively; \mathbf{F} and \mathbf{H} are the state transition and measurement matrixes, \mathbf{W} and \mathbf{V} are the system noise and measurement noise matrixes, respectively. \mathbf{F} and \mathbf{H} are written as follows:

$$\mathbf{H} = \begin{bmatrix} 1 & 0 & 0 \\ 0 & 1 & 0 \\ 0 & 0 & 1 \end{bmatrix} \quad (22)$$

$$\mathbf{F} = \begin{bmatrix} 1 & 0 & -f_k \sin\psi_k - \beta_k \cos\psi_k \\ 0 & 1 & f_k \cos\psi_k - \beta_k \sin\psi_k \\ 0 & 0 & 1 \end{bmatrix} \quad (23)$$

\mathbf{F} is updated based on the different walking patterns. Fig.7 shows the architecture of this fusion positioning system. The detailed fusion process is as follows:

(1) PDR estimates a system state:

$$\mathbf{X}(k)^- = \mathbf{F} \cdot \mathbf{X}(k-1) + \mathbf{W}(k-1) \quad (24)$$

(2) System variance matrix prediction:

$$\mathbf{P}(k)^- = \mathbf{F} \cdot \mathbf{P}(k-1) \cdot \mathbf{F}^T + \mathbf{Q}_k \quad (25)$$

where \mathbf{Q}_k is the variance of the system noise $\mathbf{W}(k)$.

(3) System observation based on geomagnetic positioning:

$$\mathbf{Z}(k) = \mathbf{H} \cdot \mathbf{G}(k) + \mathbf{V}(k) \quad (26)$$

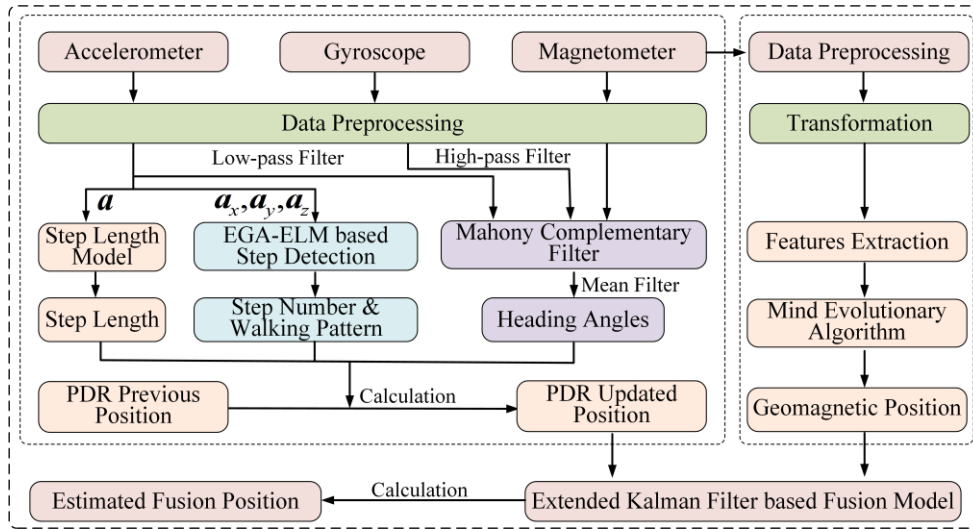


Fig. 7. The architecture of the fusion positioning system.

(4) Calculate the Kalman gain (KG):

$$\mathbf{K}(k) = \mathbf{P}(k)^- \cdot \mathbf{H}^T \cdot [\mathbf{H} \cdot \mathbf{P}(k)^- \cdot \mathbf{H}^T + \mathbf{T}_k]^{-1} \quad (27)$$

where \mathbf{T}_k is the variance matrix of $\mathbf{V}(k)$.

(5) System state is updated using KG and system observation:

$$\mathbf{X}(k) = \mathbf{X}(k)^- + \mathbf{K}(k) \cdot [\mathbf{Z}(k) - \mathbf{H} \cdot \mathbf{X}(k)^-] \quad (28)$$

(6) System variance matrix update:

$$\mathbf{P}(k) = (\mathbf{I} - \mathbf{K}(k) \cdot \mathbf{H}) \cdot \mathbf{P}(k)^- \quad (29)$$

where \mathbf{I} is an identity matrix.

IV. EXPERIMENTS

A. Experimental Setup

Experiments were carried out on the 3rd floor of the School of Environment and Spatial Informatics, China University of Mining and Technology. As Fig.8 shows, two testing paths are designed for the PDR and fusion positioning experiments. The fusion positioning software and IMU sensor data acquisition application are developed on the smartphone for testing the positioning methods and for the collection of magnetic data, respectively. During the magnetic database construction stage,

tester held on a Xiaomi 6 phone to collect data for 30 s at each reference point with a sampling rate of 50 Hz, and 380 efficient points with an interval of 1.2 m were obtained. The collected magnetic data were transformed into the GCS, features are extracted, mean values are calculated, and linearly interpolated with an interval of 0.3 m to generate a fine-grained database. 100 testing points (TP) are selected for magnetic positioning evaluation. When testing the PDR and fusion positioning, testers held the phone and walked along the reference paths, stopped at TPs for data collection. 50 TPs are selected for the localization accuracy evaluation. The errors data were analyzed using MATLAB on a laptop with an Intel Core i5-4210M CPU and 8GB RAM.

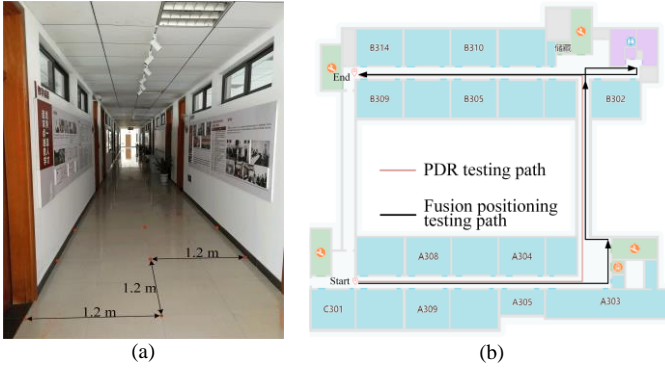


Fig. 8. Experimental area and test path. (a) realistic scenario; (b) geometric figure and testing paths.

B. Step Detection and PDR Positioning Test

1) Step detection experiment

We designed an experiment to test the EGA-ELM-based step detection algorithm. Four testers (182cm/68kg, 173cm/72kg, 180cm/75kg, and 178cm/86kg) participated in the experiment and performed different walking patterns (as Tab.I shows) by holding the smartphone horizontally. The 3-axis acceleration of different walking patterns is collected, partitioned, and labeled by using (9)-(12). Finally, 2188 training segments are obtained for model training. Then, every tester takes 100 steps for each walking pattern to obtain testing segments.

TABLE II
STEPS RECOGNITION RESULTS OF DIFFERENT USERS

Users	User 1	User 2	User 3	User 4
FM	98% (98/100)	95% (95/100)	96% (96/100)	94% (94/100)
BM	98% (98/100)	94% (94/100)	98% (98/100)	98% (98/100)
LLM	98% (98/100)	90% (90/100)	92% (92/100)	96% (96/100)
RLM	94% (94/100)	94% (94/100)	91% (91/100)	94% (94/100)
Accuracy	97% (388/400)	93.25% (373/400)	94.25% (377/400)	95.5% (382/400)
95% (1520/1600)				

Tab.II shows that the step recognition accuracy of different users varies from 93.25% to 97%. When moving forward or backward, steps can be accurately recognized with an accuracy of more than 94%, but the precision is slightly worse when moving right or left. Moreover, analyzing all the testing results, steps under different walking patterns can still be identified with a mean accuracy of 95%. Besides, based on our testing results in [45], using the same data set to build the EGA-ELM model is 4 times faster than BP and 12 times faster than CNN, which means that it is very efficient to update or use this EGA-ELM model online in the cloud or offline on the device. The testing results show the effectiveness of using EGA-ELM to detect step and prove this method can provide accurate walking pattern information for updating PDR position and prevents the PDR from wrongly updating forward.

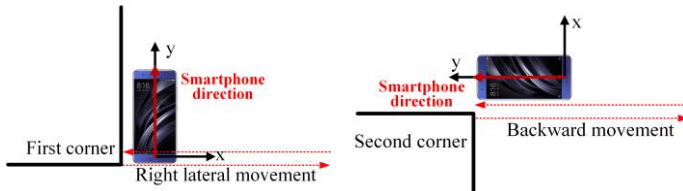


Fig. 9. Movements at two corners. (a) Move right 5 steps and return to the first corner; (b) Move back 5 steps and return to the second corner.

2) PDR test with EGA-ELM-based step detection algorithm

We carried out a simple experiment to intuitively show the detrimental influence of different walking patterns on the classic PDR model (using the FSM algorithm in [22] for step detection). Tester walked along the testing path at a constant speed but executed different movements at two path corners. The detailed walking process is presented in Fig.9 and Tab. III. Different step detection algorithms are performed on the same tracks, but the walking direction and step length estimation methods are the same. We use the FSM-based PDR and EGA-ELM-based PDR for the following discussion.

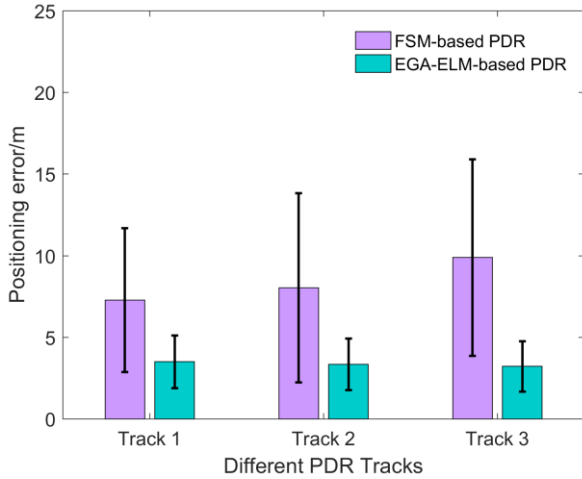
TABLE III
DETAILS OF DIFFERENT PDR TRACKS

Tracks	Walking details	Step detection algorithm
Track 1	Walk as shown in Fig.8(a) at the first corner	FSM
Track 2	Walk as shown in Fig.8(b) at the second corner	EGA-ELM
Track 3	Walk as shown in Fig.8 at two corners	

TABLE IV
POSITION ERRORS COMPARISON OF DIFFERENT PDR TRACKS

Error/(m)	FSM-based PDR			EGA-ELM-based PDR		
	Track 1	Track 2	Track 3	Track 1	Track 2	Track 3
Mean	7.28	8.03	9.89	3.22	3.34	3.50
FPDE	7.62	14.47	15.56	5.06	6.10	5.75
50% Error	8.92	5.98	10.23	2.97	3.36	3.71
90% Error	11.85	14.16	16.47	5.14	5.35	5.38

Tab. IV shows, if there is no walking patterns recognition, the mean position errors and final position drift errors (FPDEs) of the FSM-based PDR tracks are larger than those of the EGA-ELM-based PDR tracks. Under the same confidence level of 50% and 90%, FSM-based PDR shows poorer performance. Fig.10 also shows that the location accuracy of EGA-ELM-based PDR is better and the drift errors are smaller than those of the FSM-based PDR. This confirms that the classic PDR model automatically updates in the moving forward state, irrespective of the actual walking behavior. With the proposed step detection method, the movements at the two corners are successfully identified and positions are updated by using (1), reducing the drift errors. We can conclude that the proposed step detection algorithm makes PDR more error-tolerant to step identification failure.



magnetic features data at 100 testing points as the testing data and executed these four algorithms. Tab.V shows that the MEA algorithm obtains a mean location accuracy of 2.28 m, which is the best result of these four algorithms. MEA also has the lowest RMSE, 50%, and 90% errors. Fig.11 shows that there are fewer large errors when using MEA, and the red line in Fig.11 indicates that MEA has lower median positioning errors compared with the other three algorithms. We conclude that using MEA for MP can deliver good results.

TABLE V
GEOMAGNETIC POSITIONING ERRORS COMPARISON

Error/(m)	Max	Min	Mean	RMSE	50%Error	90%Error
MEA	10.59	0.10	2.28	3.31	1.52	4.52
MSD	13.11	0.31	2.53	3.52	1.69	5.50
MMFF	12.93	0.16	2.83	3.47	2.57	5.90
KNN	12.07	0.13	2.98	4.01	2.56	6.63

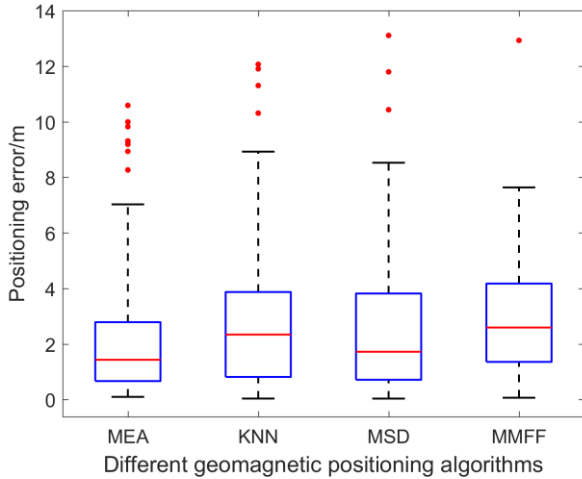


Fig. 11. Comparisons of different geomagnetic positioning methods.

Fig. 10. Positioning errors comparison of different PDR tracks.

C. Geomagnetic Positioning Test

We compare the MEA-based magnetic positioning (MP) with the KNN algorithm in [22], multi-magnetic-fingerprint-fusion (MMFF) in [32], and mean square difference (MSD) in [33]. After the magnetic database construction, we collected the

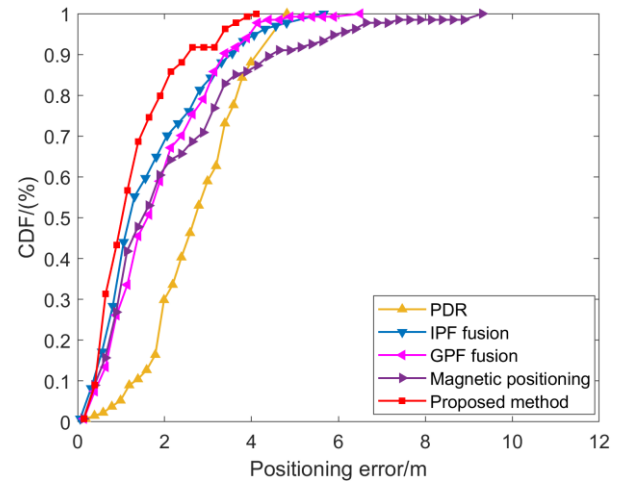


Fig. 12. CDF comparisons of different methods.

D. Fusion Positioning Methods Comparison

In this section, we analyze the performance of the proposed fusion system, and compare it to an MEA-based MP, an EGA-ELM-based PDR without MP, to the MP/PDR fusion methods using the GPF in [22] and the IPF in [35]. Both IPF and GPF have 300 particles. Tab.VI shows the positioning errors and the mean execution time (MET) for every running of these methods (Intel Core i5-4210M CPU, 8GB RAM). The mean error and RMSE of the proposed fusion method are 1.25 m and 1.53 m, respectively. These errors are lower than those of MP, PDR, IPF and GPF fusion. Moreover, under the same confidence level of 50% and 90%, the proposed system also obtains the best positioning accuracy. Fig.12 shows the cumulative distribution functions (CDF) of the errors of these five methods and it clearly shows the effectiveness of our fusion system. These results demonstrate that our fusion system can obtain high-precision localization results.

TABLE VI
POSITIONING ERRORS AND MET COMPARISON OF DIFFERENT METHODS

Method	Max (m)	Min (m)	Mean (m)	RMSE (m)	50% Error(m)	90% Error(m)	MET (s)
MP	9.31	0.15	2.12	2.79	1.51	4.42	0.119
PDR	4.82	0.19	2.70	2.89	2.67	4.06	0.002
IPF	5.66	0.15	1.64	2.06	1.16	3.55	0.377
GPF	6.49	0.14	1.81	2.16	1.61	3.38	0.379

Fig.13 presents the reconstructed trajectories of the different positioning methods. We see that the PDR position gradually deviates from the reference path over time. Our system better approximates the reference path. Although Tab.VI shows the IPF fusion and GPF fusion can give good positioning accuracy within 1.81 m, their trajectories are slightly unstable, shown by their RMSEs which exceed 2 m. This instability is caused by the unstable MP results. As a comparison, the RMSE of our system is 1.53 m. Fig.12 proves that the trajectory estimated by our system is more stable than the other three methods. Tab.VI shows that the MET of this EKF-based fusion system is about three times faster than that of IPF and GPF systems, which means that our system is computationally efficient. Combining the previous results, we conclude that fusing MEA-based MP with the EGA-ELM-based PDR based on the EKF can provide high-precision and stable positioning results.

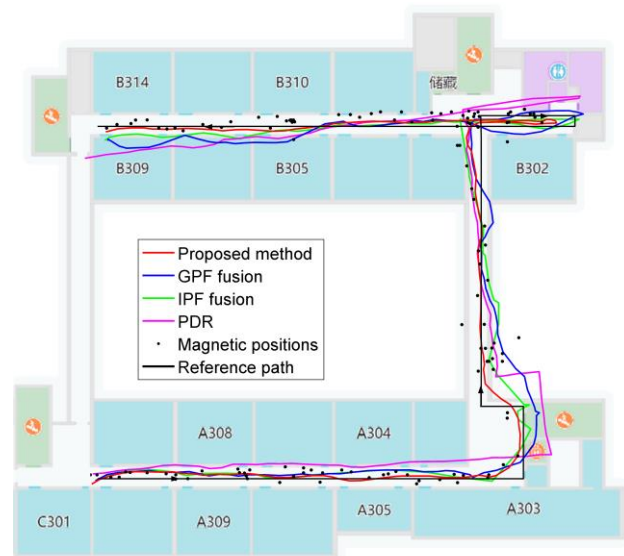


Fig. 13. Comparison of reconstructed trajectories comparison of different positioning methods.

E. Discussion

the state-of-the-art SPMPs of KNN in [22], MMFF in [32], and MSD in [33]. This MEA-based SPMP is more flexible and not restricted by walking directions and trajectories. It is easier to implement on smartphones compared with popular SBMPs in [18] and [45]. To address the error accumulation problem of PDR under different walking patterns, we design the walking pattern-based step detection method by using the EGA-ELM. Experiments reveal that the EGA-ELM-based PDR is more error-tolerant than the FSM-based PDR [22]. Compared to the similar work which uses CNN for walking patterns recognition in [12], the EGA-ELM model is lightweight and easier to construct and update.

Based on the MEA-based SPMP and EGA-ELM-based PDR, we propose a smartphone-based MP/PDR fusion model by using the EKF. This EKF-based fusion model obtains a mean accuracy of 1.25 m, which is better than that of the MP/PDR fusion approaches using GPF in [22] and IPF in [35]. Different from the popular WiFi/PDR fusion in [2], [13], PDR/Bluetooth fusion in [14], WiFi/magnetic/PDR/scene recognition fusion in [15], our method is infrastructure-free and obtains promising results. From the perspective of real-time localization, Tab.VI shows that the proposed method has a shorter localization query time than that of the IPF/GPF-based models. It is expected to run longer time on mobile phones than the fusion method in [15], which calls the camera on mobile phones will consume more battery.

Considering the positioning computational burden, accuracy, investment, our method is lightweight, infrastructure-free, and low-cost. It is more suitable to be deployed on smartphones for real-time and long-time localization in large-scale indoor environments.

V. CONCLUSION AND FUTURE WORK

This work proposed an indoor location method using mind evolutionary algorithm (MEA)-based magnetic positioning and

In this work, we concentrate on the low-accuracy problem of SPMP and propose an MEA-based SPMP, which outperforms mobile phone IMU sensors based on the EKF. Experiments showed that MEA can better excavate the true geomagnetic positions from numerous results and steps in different walking behaviors (forward, backward, sideways) can be recognized with high accuracy by using the EGA-ELM. Testing results also demonstrated that the proposed fusion method can position people with a mean accuracy of 1.25 m. However, there are still some future research directions to be deeply studied, including using multiple smartphones to test the impact of device heterogeneity on the fusion positioning method, performing the fusion method with more smartphone carrying modes, and rapid construction methods for the geomagnetic database.

REFERENCES

- [1] X. Li, X. Zhang, X. Ren, M. Fritsche, J. Wickert, and H. Schuh, "Precise positioning with current multi-constellation global navigation satellite systems: GPS, GLONASS, Galileo and BeiDou," *Sci. Rep.*, vol. 5, p. 8328, Jul.2015.
- [2] G. Chen, X. Meng, Y. Wang, Y. Zhang, P. Tian, and H. Yang, "Integrated WiFi/PDR/Smartphone using an unscented kalman filter algorithm for 3D indoor localization," *Sensors*, vol. 15, no. 9, pp. 24595-24614, 2015.
- [3] J. Trogh, D. Plets, L. Martens, and W. Joseph, "Advanced real-time indoor tracking based on the viterbi algorithm and semantic data," *Int. J. Distrib. Sens. N.*, vol. 11, no. 10, p. 271818, 2015.
- [4] J. Neburka *et al.*, "Study of the performance of RSSI based Bluetooth Smart indoor positioning," in *Proc.26th Int. Conf. Radioelektronika*, pp. 121-125, 2016.
- [5] X. Gan *et al.*, "A new array pseudolites technology for high precision indoor positioning," *IEEE Access*, vol. 7, pp. 153269-153277, 2019.
- [6] X. Zhu, J. Yi, J. Cheng, and L. He, "Adapted Error Map Based Mobile Robot UWB Indoor Positioning," *IEEE Trans. Instrum. Meas.*, vol.69, no.9, pp.6336-6350, Step. 2020.
- [7] S. Seol, E.-K. Lee, and W. Kim, "Indoor mobile object tracking using RFID," *Future Generat. Comput. Syst.*, vol. 76, pp. 443-451, Nov. 2017.
- [8] S.-H. Fang, C.-H. Wang, T.-Y. Huang, C.-H. Yang, and Y.-S. Chen, "An enhanced ZigBee indoor positioning system with an ensemble approach," *IEEE Commun. Lett.*, vol. 16, no. 4, pp. 564-567, Apr. 2012.
- [9] Y. Chen, R. Chen, M. Liu, A. Xiao, D. Wu, and S. Zhao, "Indoor visual positioning aided by CNN-based image retrieval: Training-free, 3D

- modeling-free," *Sensors*, vol. 18, no. 8, p. 2692, Aug. 2018.
- [10] C. Cadena *et al.*, "Past, present, and future of simultaneous localization and mapping: Toward the robust-perception age," *IEEE Trans. Robot.*, vol. 32, no. 6, pp. 1309-1332, 2016.
- [11] I. Ashraf, S. Hur, and Y. J. E. Park, "Smartphone sensor based indoor positioning: current status, opportunities, and future challenges," *Electronics*, vol. 9, no. 6, p. 891, 2020.
- [12] Q. Wang *et al.*, "Pedestrian Dead Reckoning based on Walking Pattern Recognition and Online Magnetic Fingerprint Trajectory Calibration," *IEEE Internet. Things J.*, vol.8, pp.2011-2026, Feb.2021.
- [13] C. De Cock, W. Joseph, L. Martens, J. Trogh, and D. Plets, "Multi-Floor Indoor Pedestrian Dead Reckoning with a Backtracking Particle Filter and Viterbi-Based Floor Number Detection," *Sensors*, vol. 21, no. 13, p. 4565, May. 2021.
- [14] X. Li, J. Wang, and C. J. S. Liu, "A Bluetooth/PDR integration algorithm for an indoor positioning system," *Sensors*, vol. 15, no. 10, pp. 24862-24885, Sep. 2015.
- [15] M. Liu *et al.*, "Scene recognition for indoor localization using a multi-sensor fusion approach," *Sensors*, vol. 17, no. 12, p. 2847, 2017.
- [16] B. Li, T. Gallagher, A. G. Dempster, and C. Rizos, "How feasible is the use of magnetic field alone for indoor positioning?," in *Proc. IPIN*, vol.13, 2012, pp.1-15.
- [17] S. Suksakulchai, S. Thongchai, D. M. Wilkes, and K. Kawamura, "Mobile robot localization using an electronic compass for corridor environment," in *Proc. SMC Conf. IEEE Int. Conf. Syst., Man Cybern, Cybern. Evolving Syst., Hum., Org., Complex Interact.*, Nashville, TN,USA, 2000, pp. 3354-3359.
- [18] J. Kuang, X. J. Niu, P. Zhang, and X. G. Chen, "Indoor Positioning Based on Pedestrian Dead Reckoning and Magnetic Field Matching for Smartphones," *Sensors*, vol. 18, no. 1, p. 1-21, Nov. 2018.
- [28] I. Ashraf, S. Hur, and Y. Park, "mPILOT-Magnetic Field Strength Based Pedestrian Indoor Localization," *Sensors*, vol. 18, no. 7, p. 2283, Jul 2018.
- [29] I. Ashraf, S. Hur, M. Shafiq, S. Kumari, and Y. Park, "GUIDE: Smartphone sensors-based pedestrian indoor localization with heterogeneous devices," *Int. J. Commun. Syst.*, vol. 32, no. 15, p. e4062, 2019.
- [30] B. Bhattarai, R. K. Yadav, H.-S. Gang, and J.-Y. Pyun, "Geomagnetic Field Based Indoor Landmark Classification Using Deep Learning," *IEEE Access*, vol. 7, pp. 33943-33956, 2019.
- [31] S.-C. Yeh, W.-H. Hsu, W.-Y. Lin, and Y.-F. Wu, "Study on an Indoor Positioning System Using Earth's Magnetic Field," *IEEE Trans. Instrum.Meas.*, vol.63,no.3,pp.865-872, Mar.2020.
- [32] G.-X. Liu, L.-F. Shi, S. Chen, and Z.-G. Wu, "Focusing Matching Localization Method Based on Indoor Magnetic Map," *IEEE Sensors J.*, vol.20,no.17, pp.10012-10020, Sep. 2020.
- [33] R. Kang and L. Cao, "Smartphone indoor positioning system based on geomagnetic field," in *Proc. Chin. Autom. Congr. (CAC), Oct. 2017*, pp. 1826-1830.
- [34] H. Huang, W. Li, D. A. Luo, D. W. Qiu, and Y. Gao, "An Improved Particle Filter Algorithm for Geomagnetic Indoor Positioning," *J. Sensors*, vol. 2018, pp.1-9, Mar.2018.
- [35] M. Zhang, T. Qing, J. Zhu, and W. J. I. J. o. D. S. N. Shen, "Indoor positioning tracking with magnetic field and improved particle filter," *Int. J. Distrib. Sens. N.*, vol. 13, no. 11, p. 1550147717741835, 2017.
- [36] A. Manos, I. Klein, and T. Hazan, "Gravity direction estimation and heading determination for pedestrian navigation," in *Proc. Int. Conf. IPIN*, pp. 206-212, Sep.2018.
- [37] R. Zhou, "Pedestrian dead reckoning on smartphones with varying walking speed," in *Proc. ICC. May. 2016*, pp. 1-6.
- [38] A. Poulouse, B. Senouci, and D. S. Han, "Performance Analysis of Sensor Fusion Techniques For Heading Estimation Using Smartphone Sensors," *IEEE Sensors J.*, vol.19, n0.24, pp. 12369- 12380, Dec. 2019.
- [39] B. Shin *et al.*, "Motion recognition-based 3D pedestrian navigation system using smartphone," *IEEE Sensors J.*, vol. 16, no. 18, pp. 6977-6989, Sep. 2016.
- [40] R. Mahony, T. Hamel, and J.-M. Pflimlin, "Nonlinear Complementary Filters on the Special Orthogonal Group," *IEEE Trans. Autom. Control.*, vol. 53, pp. 1203-1218, Jun. 2008.
- [41] D. Ahn *et al.*, "A design of the low-pass filter using the novel microstrip defected ground structure," *IEEE Trans. Microw. Theory Techn.*, vol. 49, no. 1, pp. 86-93, Jan.2001.
- [42] L. Keselbrener, M. Keselbrener, and S. Akselrod, "Nonlinear high pass filter for R-wave detection in ECG signal," *Med. Eng. Phys.*, vol. 19, no. 5, pp. 481-484, Jun. 1997.
- [19] K. P. Subbu, B. Gozick, and R. Dantu, "LocateMe: Magnetic-fields-based indoor localization using smartphones," *ACM Trans. Intel. Syst.Technol.*, vol. 4, no. 4, p. 73, 2013.
- [20] I. Ashraf, M. Kang, S. Hur, and Y. Park, "MINLOC: Magnetic Field Patterns-Based Indoor Localization Using Convolutional Neural Networks," *IEEE Access*, vol. 8, pp. 66213-66227, 2020.
- [21] H. J. Bae and L. Choi, "Large-Scale Indoor Positioning using Geomagnetic Field with Deep Neural Networks," in *Proc. IEEE Int. Conf. Commun.(ICC)*, May 2019, pp. 1-6.
- [22] M. Sun, Y. Wang, S. Xu, H. Cao, and M. Si, "Indoor Positioning Integrating PDR/Geomagnetic Positioning Based on the Genetic-Particle Filter," *Appl. Sci.*, vol. 10, no. 2, p. 668, Jan. 2020.
- [23] L. Hou *et al.*, "Orientation-Aided Stochastic Magnetic Matching for Indoor Localization," *IEEE Sensors J.*, vol. 20, no. 2, pp. 1003-1010, Jan. 2020.
- [24] H. Xie, T. Gu, X. Tao, H. Ye, and J. Lu, "A reliability-augmented particle filter for magnetic fingerprinting based indoor localization on smartphone," *IEEE Trans. Mobile Comput.*, vol. 15, no. 8, pp. 1877-1892, Aug. 2016.
- [25] M. Zheng, Y. Zhao, Y. He, and C.-Z. Xu, "Sensitivity-based adaptive particle filter for geomagnetic indoor localization," in *Proc. IEEE/CIC Int. Conf. Commu. China (ICCC)*, Qingdao, China, Oct. 2017, pp. 1-6.
- [26] K. P. Subbu, B. Gozick, and R. Dantu, "Indoor localization through dynamic time warping," in *2011 Proc. Syst., Man, Cybern.(SMC)*, Anchorage, AK,USA,Oct. 2011, pp. 1639-1644.
- [27] Y. Shu, C. Bo, G. Shen, C. Zhao, L. Li, and F. Zhao, "Magicol: Indoor localization using pervasive magnetic field and opportunistic WiFi sensing," *IEEE J. Sel. Areas Commun.*, vol. 33, no. 7, pp. 1443-1457, Jul. 2015.
- [43] E. Buckwar and M. G. Riedler, "Runge-Kutta methods for jump-diffusion differential equations," *J. Comput. Appl. Math.*, vol. 236, no. 6, pp. 1155-1182, Oct.2011.
- [44] H. Xia, J. Zuo, S. Liu, and Y. Qiao, "Indoor localization on smartphones using built-in sensors and map constraints," *IEEE Trans. Instrum.Meas.*, vol. 68, no. 4, pp. 1189-1198, 2018.
- [45] M. Sun, Y. Wang, S. Xu, H. Yang, and K. Zhang, "Indoor Geomagnetic Positioning Using the Enhanced Genetic Algorithm based Extreme Learning Machine," *IEEE Trans. Instrum.Meas.*, vol.70, pp.1-11, 2021.
- [46] E. Vildjiounaite, E.-J. Malm, J. Kaartinen, and P. Alahuhta, "Location estimation indoors by means of small computing power devices, accelerometers, magnetic sensors, and map knowledge," in *Pervasive Computing (Lecture Notes in Computer Science)*, vol. 2414. Berlin, Germany: Springer, Jan. 2002, pp. 211-224.
- [47] Q. Ladetto, "On foot navigation: continuous step calibration using both complementary recursive prediction and adaptive Kalman filtering," in *Proc. ION GPS*, vol. 2000, pp. 1735-1740,2000.
- [48] Q. Tian, Z. Salcic, I. Kevin, K. Wang, and Y. Pan, "A multi-mode dead reckoning system for pedestrian tracking using smartphones," *IEEE Sens. J.*, vol. 16, no. 7, pp. 2079-2093, 2015.
- [49] H. Weinberg, "Using the ADXL202 in pedometer and personal navigation applications," *Analog Devices Appl. Notes AN-602*, 2002, pp. 1-6, vol. 2.
- [50] F. Gu, K. Khoshelham, C. Yu, and J. Shang, "Accurate step length estimation for pedestrian dead reckoning localization using stacked autoencoders," *IEEE Trans. Instrum.Meas.*, vol.68, pp2705-2713, Aug. 2019.
- [51] S. Chengyi, S. Yan, and X. Keming, "Mind-evolution-based machine learning and applications," in *Proc. 3rd World Congress on Intelligent Control and Automation (WCICA 2000)*, pp. 112-117, June 28-July 2, 2000.
- [52] R. Malhotra, N. Singh, and Y. Singh, "Genetic algorithms: Concepts, design for optimization of process controllers," *Comput. Inf. Sci.*, vol. 4, no. 2, pp. 39-54, 2011.